# Performance of Time-Domain Line Protection Elements on Real-World Faults

Edmund O. Schweitzer, III, Bogdan Kasztenny, and Mangapathirao V. Mynam
*Schweitzer Engineering Laboratories, Inc.*



This paper was presented at the 69th Annual Conference for Protective Relay Engineers and can be accessed at: https://doi.org/10.1109/CPRE.2016.7914904.

For the complete history of this paper, refer to the next page.

Published in
*Locating Faults and Protecting Lines at the Speed of Light: Time-Domain Principles Applied*, 2018

Previously presented at the
3rd Annual PAC World Americas Conference, August 2016,
70th Annual Georgia Tech Protective Relaying Conference, April 2016,
and 69th Annual Conference for Protective Relay Engineers, April 2016

Previous revised edition released October 2015

Originally presented at the
42nd Annual Western Protective Relay Conference, October 2015

# Performance of Time-Domain Line Protection Elements on Real-World Faults

Edmund O. Schweitzer, III, Bogdan Kasztenny, and Mangapathirao V. Mynam,
*Schweitzer Engineering Laboratories, Inc.*

***Abstract*—Ultra-high-speed line protection is becoming a reality today, giving the industry a way to trip line faults in a few milliseconds. One relay described in this paper that uses time-domain principles incorporates incremental-quantity (TD32) and traveling-wave (TW32) directional elements in a communications-assisted tripping scheme, incremental-quantity distance element (TD21), and traveling-wave differential element (TW87). This paper introduces these time-domain line protection elements, shares key details of their implementation in hardware, and illustrates their operation using real-world faults and digital simulations. By comparing the performance of the time-domain line protection elements with the traditional phasor-based elements of the in-service relays that captured the fault records, we demonstrate the performance of the time-domain line protection elements.**

## I. Introduction

Since the earliest days of electric power, engineers have continually improved protection as measured by speed, sensitivity, dependability, security, and selectivity. Today, time-domain relays are becoming available for ultra-high-speed line protection. These relays use traveling-wave (TW) principles as well as tried-and-true incremental-quantity principles to provide ultra-high-speed and secure line protection. High sampling rates, data storage, processing power, and communications capabilities of new relay hardware platforms allow us to improve line protection operating times [1] and fault locating [2] [3] [4].

Section II of this paper briefly reviews the theory and implementation of our time-domain line protection elements. These elements are an incremental-quantity directional element (TD32) and a TW directional element (TW32) in a permissive overreaching transfer tripping (POTT) scheme, an incremental-quantity distance element (TD21), and a TW line current differential element (TW87).

Section III demonstrates the performance of the incremental-quantity-based line protection elements using a number of field events. These real-world events include internal faults on several transmission lines of various voltage levels, lengths, source-to-impedance ratios, series compensations, coupling-capacitor voltage transformers (CCVTs), and other factors. Utilities have captured these events using in-service relays with high sampling rates and TW fault locators. We use the performance of the traditional phasor-based directional and distance elements of the in-service relays as a base for comparing the performance of the TD32 and TD21 line protection elements.

Section IV illustrates the performance of the TW-based line protection elements, TW32 and TW87, using digital simulations. We also use a field case captured by the TW fault locator to show the performance of the TW87 element.

In Section V, we compare the performance of the incremental-quantity-based protection elements (TD21 and TD32) with two line relays that use phasor-based principles.

## II. Review of Time-Domain Line Protection Elements

This section summarizes the theory of time-domain line protection elements and presents key details of our implementation (patent pending). These details allow better understanding and appreciation of the analysis and results that follow.

### A. Key Signals and Settings

We start by listing key signals and settings common to our line protection elements. Reference [1] contains more details on the theory and calculation of these signals.

| | |
|---|---|
| $v_\Phi$ | relay phase-to-ground voltage, phase Φ. |
| $i_\Phi$ | relay phase current, phase Φ. |
| $v$ | loop voltage. |
| $i$ | loop current. |
| $\Delta v$ | loop incremental voltage. |
| $\Delta i$ | loop incremental current. |
| $\Delta i_Z$ | loop incremental replica current. |
| $v_{TW}$ | voltage traveling wave. |
| $i_{TW}$ | current traveling wave. |
| $Z_1$, $Z_0$ | line positive- and zero-sequence impedances. |
| $m_0$ | TD21 reach in per unit. |
| $Z_F$, $Z_R$ | TD32 forward and reverse impedance thresholds. |
| $T_L$ | line propagation time. |
| P | pickup of the TW87 element. |

### B. Signal Acquisition and Processing

Fig. 1 presents a simplified signal acquisition diagram of our time-domain relay. We sample line currents and voltages at the rate of 1 MHz, suitable for TW protection and fault locating. The samples are aligned with an absolute time input of the relay for convenient event analysis and fault locating. We apply an analog low-pass filter to avoid signal aliasing and use a simple differentiator-smoother filter [2] to extract traveling waves from the raw currents and voltages. We decimate the 1 MHz samples to the 10 kHz rate for processing the incremental-

quantity-based algorithms. We apply a digital anti-aliasing filter to avoid aliasing at the 10 kHz rate.

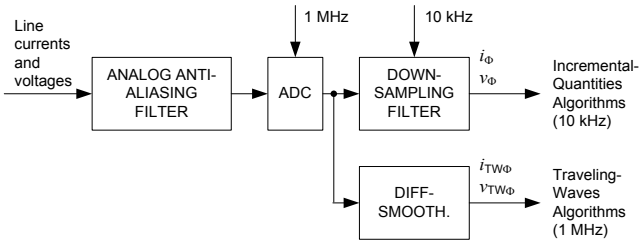


Fig. 1. Simplified data acquisition diagram for incremental-quantity and TW protection algorithms.

Fig. 2a presents the differentiator-smoother data window and Fig. 2b illustrates its operation. Considered over a period of a few tens of microseconds, the current is quasi constant (i.e., changing very slowly). A TW is a sharp change from one quasi-steady level to a different quasi-steady level. The differentiator-smoother filter responds to an ideal step change with a triangle-shaped output, and it responds to a ramp transition between two levels with a parabola-shaped output. We use the time associated with the peak of the output as the TW arrival time, factoring a constant group delay of half the differentiator-smoother window length. We select the gain of the differentiator-smoother filter so that the peak value of the output corresponds to the magnitude of the step change in the input. This way our TW signals retain information about the magnitude of the TWs.

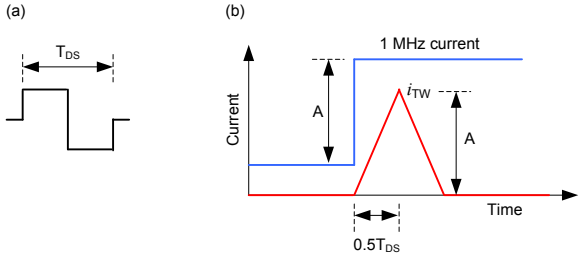


Fig. 2. Differentiator-smoother data window (a) and operation (b).

Fig. 3 depicts an integrator—a common block we use in our time-domain line protection elements. The function of an integrator is to add or accumulate input values. An integrator can be seen as a counterpart to a phasor estimator in phasor-based relays. An integrator is well suited for incremental quantities or TWs because these signals are ideally zero prior to an event. An integrated signal is a proxy for a confidence level in measured signals because the energy of the input signal accumulates over time. Integrating a signal that develops from zero does not slow down decisions based on the integrated signal when comparing two or more of such signals.

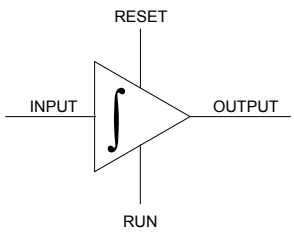


Fig. 3. Security integrator with control inputs.

In our implementation, the integrator has two control inputs (RUN and RESET) that control its behavior under different operating conditions. We use carefully designed logic to decide when any given integrator can accumulate its input signal.

### C. Traveling-Wave Directional Element (TW32)

References [1], [2], and [5] explain the fundamentals of using voltage and current TWs for fault direction discrimination. Theoretically, we need a wide-bandwidth (high-fidelity) voltage transformer to measure voltage TWs. However, in most cases we can measure the first voltage TW even with a CCVT (because of interwinding capacitance across the step-down transformer and the interturn capacitance across the tuning reactor of the CCVT). This voltage TW measurement is not accurate in terms of voltage TW magnitude, but it is accurate in terms of the arrival time and polarity. This timing and polarity accuracy is sufficient for the TW32 element.

We use phase voltage and current TWs as shown in Fig. 4. We calculate the TW torque as a product of the TW current and the sign-inverted TW voltage (so the torque is positive for forward events). We integrate the torque over time. For security, we release the integrator only if both the voltage and current TWs are above minimum levels. We check the output of the integrator ($E_{FWD}$) after time T1 (in the order of tens to hundreds of microseconds) from the beginning of the disturbance. We assert the TW32 output when $E_{FWD}$ exceeds a security margin.

Each TW coming from the line direction will integrate up, and each TW coming from behind the relay will integrate down. The first TW is higher in magnitude than the subsequent reflections. As a result, we have confidence that the integrated value is a reliable indication of the fault direction even as multiple reflected TWs are integrated over the time period T1.

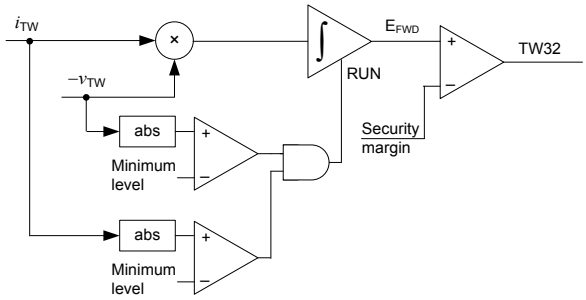


Fig. 4. Simplified logic of the TW32 element.

We run three TW32 elements for the three phases.

### D. Traveling-Wave Differential Element (TW87)

Reference [1] derives our TW line current differential protection principle. This element compares timing, polarities and magnitudes of current TWs at both terminals of the line. For an external event, the current TW enters at one line terminal and, after the line propagation time, leaves at the other terminal with the opposite polarity but not necessarily with the same magnitude [6].

We implement the principle as follows. First, we identify the time (as a sample index) of the first TW at both the local and

remote terminals. For the local and remote terminals, we label these two indices $NL_{FIRST}$ and $NR_{FIRST}$, respectively. Finding these indices is not difficult, because these are the first waves recorded after the quiescent steady state prior to the disturbance.

Second, knowing the index of the first TW at the local terminal, we establish a time window to detect the exiting TW at the remote terminal. Similarly, knowing the index of the first TW at the remote terminal, we establish the time window to detect the exiting TW at the local terminal. These windows are positioned at the nominal line propagation time, $T_L$, following the first TW. We also need to include a margin, $\Delta T_L$, for the error and variability in the propagation time (to accommodate conditions such as conductor sagging).

Third, we inspect the TW recording in the TW exit time interval and identify the maximum absolute value in that time interval. We label the index of that maximum value identified by the local and remote relays as the exit index $NL_{EXIT}$ and $NR_{EXIT}$, respectively. Fig. 5 shows the first TW at the local terminal and the exit TW at the remote terminal.

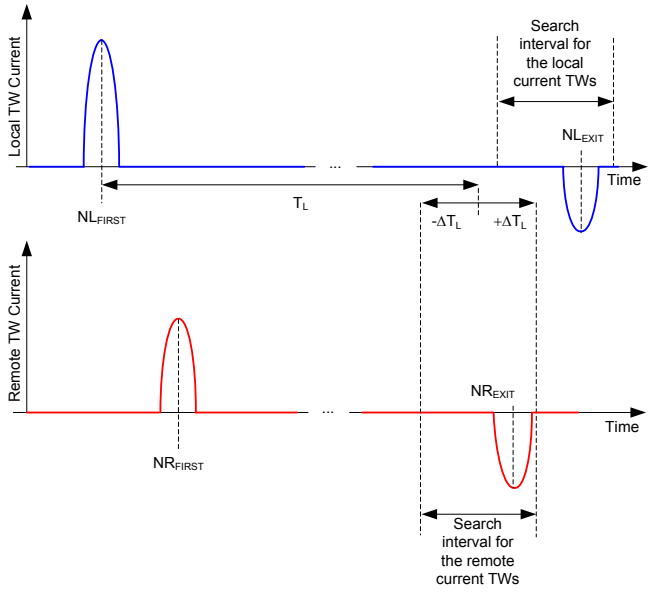


Fig. 5. Defining the FIRST and EXIT TWs for the TW87 element.

After identifying the four indices, we calculate the following signals, using M samples in the order of one half of the differentiator smoother window ($M < 0.5 \cdot T_{DS}$).

Magnitudes of the first current TWs:

$$IL = C \cdot \left| \sum_{k=-M}^{k=M} i_{TWL(NL_{FIRST}-k)} \right| \quad (1a)$$

$$IR = C \cdot \left| \sum_{k=-M}^{k=M} i_{TWR(NR_{FIRST}-k)} \right| \quad (1b)$$

We selected the scaling factor C to maintain a unity gain in the values of (1) for an ideal step TW.

Operating TW current:

$$I_{DIF} = C \cdot \left| \sum_{k=-M}^{k=M} \left( i_{TWL(NL_{FIRST}-k)} + i_{TWR(NR_{FIRST}-k)} \right) \right| \quad (2)$$

Restraining TW current:

If $NL_{FIRST} < NR_{FIRST}$,

$$I_{RST} = C \cdot \left| \sum_{k=-M}^{k=M} \left( i_{TWL(NL_{FIRST}-k)} - i_{TWR(NR_{EXIT}-k)} \right) \right| \quad (3a)$$

else,

$$I_{RST} = C \cdot \left| \sum_{k=-M}^{k=M} \left( i_{TWR(NR_{FIRST}-k)} - i_{TWL(NL_{EXIT}-k)} \right) \right| \quad (3b)$$

Fault location:

$$m_{87} = 0.5 \left( 1 + \frac{NL_{FIRST} - NR_{FIRST}}{T_L} \right) \quad (4)$$

After calculating (1) through (4), we apply the TW87 logic shown in Fig. 6.

We run three TW87 elements, one for each phase. Any fault type would excite at least two conductors with current TWs. For security, we require all phase elements with local, remote, and operating currents greater than their corresponding pickup level to declare an internal fault condition before we allow the TW87 to assert its output.

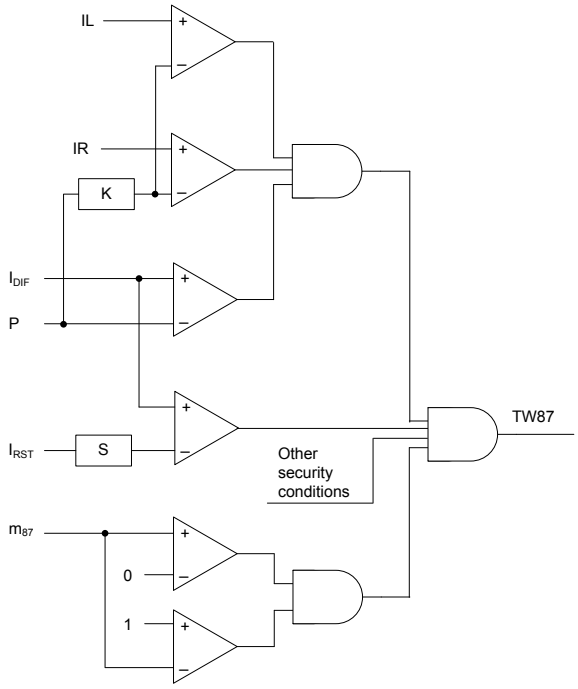


Fig. 6. Simplified TW87 logic (P–minimum pickup, S–slope, K–minimum TW factor).

Any sudden voltage change at a point on the protected line launches TWs [7]. Such changes include switching in-line series capacitors and reactors or a shield wire lightning strike.

Therefore, the TW87 logic requires additional supervision conditions for security.

### *E. Incremental-Quantity Filtering and Signal Processing*

Fig. 7 presents common calculations for our incremental-quantity-based protection elements. We show only the current path; the voltage path is identical except for a lack of replica values. The theory of these quantities is well known; see [1] for details. We offer the following comments to aid understanding of our implementation:

- Using BUFFER-2 in Fig. 7, we calculate the incremental line currents ($\Delta i_\Phi$) by subtracting one-period-old values from the line currents ($i_\Phi$). These signals receive no additional low-pass filtering and, therefore, incur no extra delay. We use these signals in the TD32 element for an initial boost in speed and security during the first millisecond of a fault.
- We calculate six loop replica currents ($i_Z$) from the line currents, taking into account the three-phase nature of the protected line and the L/R ratios of the six measurement loops (three phase-to-ground loops and three phase-to-phase loops). We extract the 3x3 R and L matrices necessary for these calculations from the magnitudes and angles of the positive- and zero-sequence line impedances.
- Using BUFFER-1 in Fig. 7, we calculate the loop incremental replica currents ($\Delta i_Z$) by subtracting the one-period-old values.
- Finally, we apply low-pass filters (LPF) to control transients in our operating signals.
- The filters labeled as LF (lower frequency) pass signals in the range of hundreds of hertz. This level of filtering is required to achieve a desired reach accuracy of the TD21 element. The filter labeled HF (higher frequency) passes signals in the range of 1 kHz. This relaxed level of filtering is suitable for the TD32 element, because it does not need to control its reach.

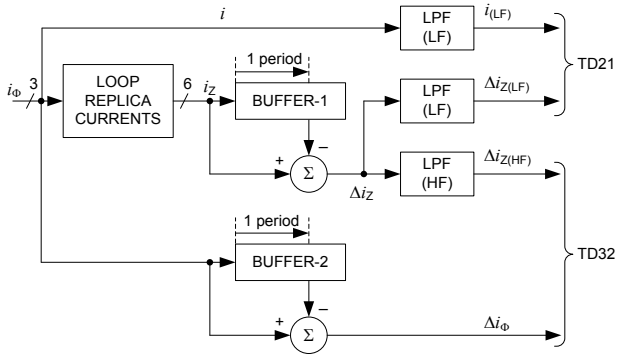


Fig. 7. Simplified filtering for the incremental-quantity algorithms (current path).

### *F. Incremental-Quantity Directional Element (TD32)*

Reference [1] derives the theory of the TD32 element. We base the element on a torque, i.e., a product of the instantaneous incremental voltage and the instantaneous incremental replica current. We apply adaptive restraints for the operating torque using the well-known concept of the threshold impedances [1] [8]. As shown in Fig. 8, we calculate the operating torque using a sign-inverted voltage so that the operating torque, $T_{OP}$, is positive for forward events. The two restraining torques are proportional to the product of the squared loop replica current and the corresponding threshold impedance magnitudes. We use a positive restraining torque, $T_{FWD}$, for checking the forward direction, and we use a negative restraining torque, $T_{REV}$, for checking the reverse direction. We use the HF filter in the loop quantities to provide speed for the TD32 element. We run identical calculations for all six loops.

The calculations on the right side of Fig. 8 provide an initial boost in the operating torque and in one of the restraining torques. This boost comes from the loop incremental voltages ($\Delta v_\Phi$) and currents ($\Delta i_\Phi$). We know that for a very short period of time (submillisecond) the incremental voltage and current are of opposite polarities for a forward event and of the same polarity for a reverse event [1]. The torque ($-\Delta v_\Phi \cdot \Delta i_\Phi$) is applied for a short period of time, T2, following disturbance detection (a fraction of a millisecond).

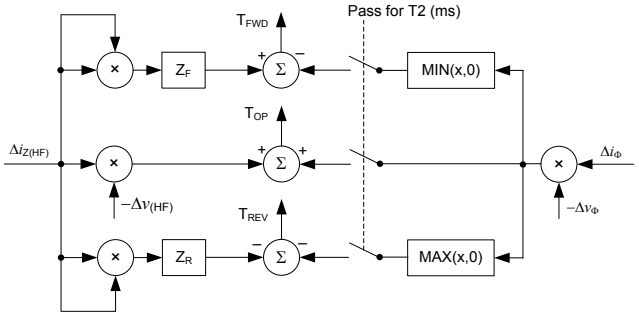


Fig. 8. TD32 torque calculations.

We integrate the torques ($T_{OP}$, $T_{FWD}$, $T_{REV}$) as shown in Fig. 9 and use security margins to shift the integrated restraining values away from zero. Finally, we compare the integrated operating torque with the adaptive integrated restraining torques and declare the forward or reverse direction.

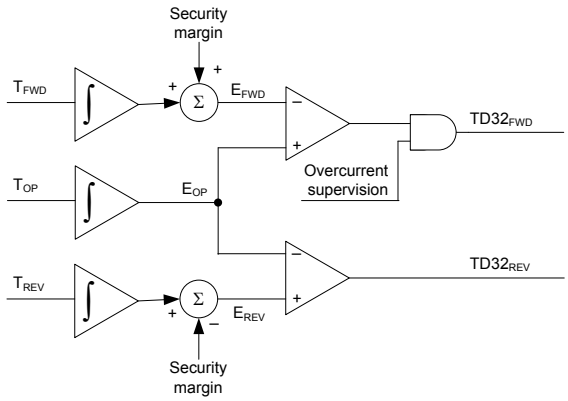


Fig. 9. TD32 torque integration and comparison.

The outputs of Fig. 9 are further conditioned according to the fault type for their application in the permissive scheme and for supervision of the TD21 element.

### G. Incremental-Quantity Distance Element (TD21)

Reference [1] derives the theory of the TD21 element based on the fundamentals [9]. The principle compares the calculated voltage change at the intended reach point (operating voltage, $V_{21OP}$) with the prefault voltage at the reach point (restraining voltage, $V_{21RST}$). For a fault at the reach point, the highest change in the voltage is when the prefault voltage collapses all the way to zero (a bolted fault, $R_F = 0$). If the change is higher ($V_{21OP} > V_{21RST}$), the fault must be between the relay and the reach point and the element asserts.

We calculate the TD21 operating voltage on a per loop basis using the lower frequency spectrum in the incremental signals:

$$V_{21OP} = \Delta v_{(LF)} - m_0 \cdot |Z_1| \cdot \Delta i_{Z(LF)} \quad (5)$$

We use the concept of a point-on-wave restraint by calculating the instantaneous voltage at the reach point. We use the signals filtered at the lower frequency to match the filtering for the operating voltage:

$$V_{21R} = v_{(LF)} - m_0 \cdot |Z_1| \cdot i_{Z(LF)} \quad (6)$$

We know that the restraining voltage calculated with (6) is not perfectly accurate [1]. Nonetheless, (6) is a good approximation of the actual voltage at the reach point. Of course, we need the prefault value of (6) to represent the voltage at the reach point prior to the fault.

Fig. 10a presents our implementation. We multiply the absolute value of the restraint voltage (6) by the factor k and buffer it. Factor k is slightly above 1 for security purposes. We extract one-period-old data and two extra sets of data: one ahead and one beyond the exact one-period-old data. The maximum value among the minimum restraint level and the three values becomes the final TD21 restraint, $V_{21RST}$. We use the minimum restraint level to enforce the minimum TD21 restraint for points on wave near the zero crossings (i.e., for time intervals when the restraining signal is very small or zero).

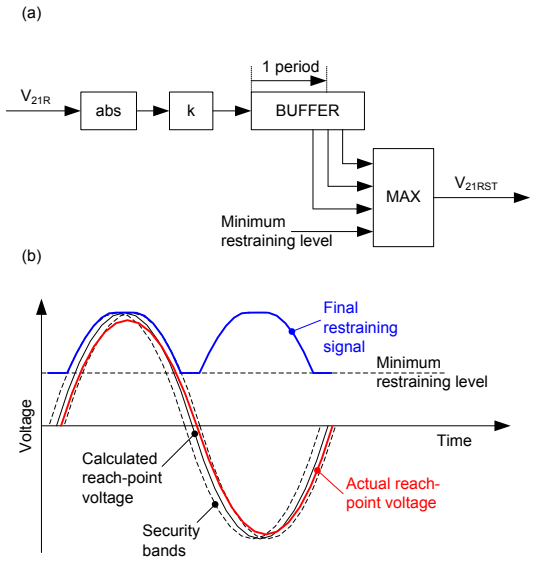


Fig. 10. Calculations of the point-on-wave TD21 restraining signal: logic diagram (a) and example of operation (b).

Fig. 10b illustrates the calculation of the TD21 restraining voltage. Our goal is to create a signal that envelops the actual reach point voltage while assuming various sources of errors, yet is as small as possible to improve speed and sensitivity. We refer to the restraint of Fig. 10 as a point-on-wave restraint to contrast it with a constant worst-case value of the nominal system voltage plus margin.

After calculating the operating and restraining signals, we compare them as shown in Fig. 11. We determine if the operating signal is above the restraining signal by integrating the difference between the two signals. We run the integrator if the loop is involved in the fault and if the incremental voltage at the reach point resulted from a voltage decrease (collapse). In general, the incremental voltage at the reach point may result from any voltage change, either a voltage decrease or increase. We allow the TD21 to integrate only if the voltage has collapsed. We confirm the collapse by checking the relative polarity of the restraining voltage, $V_{21R}$, prior to the fault against the operating voltage, $V_{21OP}$. The incremental voltage at the fault should be negative for a positive restraining voltage and vice versa. This check provides extra security against switching events. By running this check, the TD21 element effectively responds to the signed restraining voltage, not the absolute value of it.

We run the TD21 integrator starting from the time the absolute value of the operating signal is above the restraining signal. The TD21 element asserts ($TD21_{PKP}$) if the integrated difference is above the security margin and if the loop incremental replica current is above a threshold (overcurrent supervision).

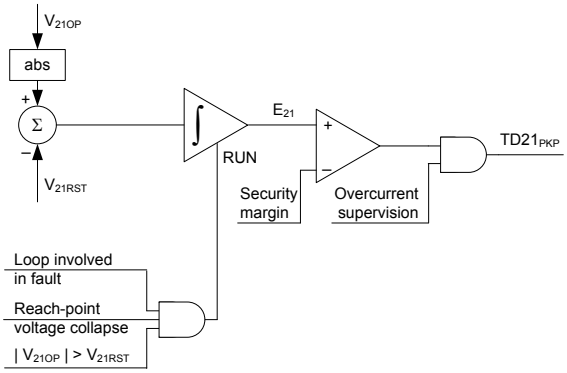


Fig. 11. TD21 integration and comparison.

## III. Performance on Incremental-Quantity-Based Line Protection for Selected Field Cases

This section uses real-life events recorded by in-service line protective relays sampling at adequate rates to illustrate the time-domain line protection principles and to compare their performance with the in-service relays. These relays use full-cycle phasor-based elements and some of them use half-cycle and full-cycle phasor-based elements.

We resampled the field records to match the sampling rates of the new algorithms (1 MHz for the TW principles and 10 kHz for the incremental-quantity principles). In some of the cases, we needed to up-sample the data. As a result, in this section, we are using currents and voltages with the high-

frequency content reduced by applying the anti-aliasing filter prior to storing the signals in the in-service relays, which is at a rate lower than 10 kHz.

Table I lists the field cases that we evaluated and compares the response times of the new protection elements with the in-service relays. The TD32 and TD21 elements show significant speed advantage over the phasor-based directional (PH32) and distance (PH21) elements of the in-service relays. In the following text, we share details about a few selected cases.

### *A. Case 1 and Case 2: Double-Line-to-Ground Close-In Fault*

A C-phase-to-A-phase-to-ground (CAG) close-in (0.18 pu) fault struck a 159 km, 230 kV line connected to a strong system with a positive-sequence source-to-line impedance ratio (SIR) of 0.13. The in-service relay asserted its forward directional element in 7.6 ms and tripped from distance Zone 1 in 9.6 ms. The TD32 and TD21 elements responded in 2.3 ms and 2.8 ms, respectively (Fig. 12).

Fig. 13 shows the incremental voltage and current for the CA loop. Note that the current starts changing at about 1 ms into the fault, and this has an effect on the response time of both the incremental-quantity and phasor-based elements. The incremental voltage and the replica incremental current are of opposite polarities as expected, despite the difference in the L/R ratios for the line and the system. As a result, the TD32 operating torque is decisively positive (Fig. 14). The integrated operating torque exceeds the forward restraining torque in a fraction of a millisecond. The TD32 element operates slightly later, when its overcurrent supervision asserts. Fig. 14 clearly shows the initial boost in the operating torque resulting from the usage of the incremental voltage ($\Delta v_{\Phi}$) and current ($\Delta i_{\Phi}$). Fig. 14 illustrates both the TD32 dependability (the operating torque is much higher than the positive, forward restraining torque) and security (the operating torque is well above the negative, reverse restraining torque).

Fig. 15 shows the operating and restraining voltages of the TD21 element and the integrated voltage difference. For this close-in fault, the TD21 element operates very fast (1.9 ms) with a large dependability margin (the peak operating voltage is twice the peak restraining voltage).

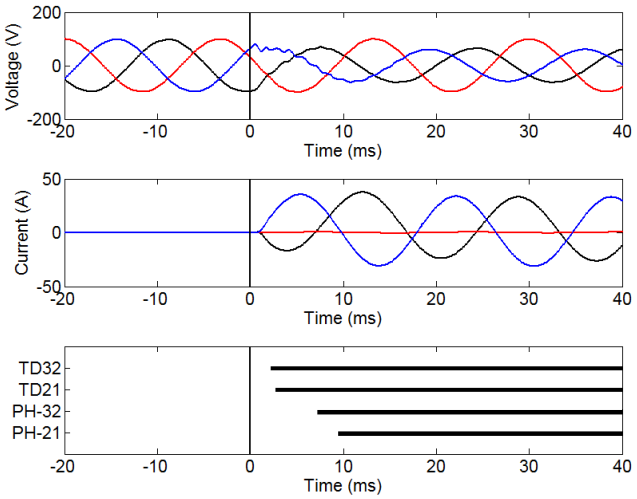


Fig. 12. Case 1: Relay secondary voltage and current and the outputs of the directional and underreaching elements.

Case 2 is the same fault, but seen from the remote line terminal. From the remote terminal point of view, this fault is just outside of the TD21 reach. Therefore, TD21 does not

TABLE I
FIELD CASES USED FOR PERFORMANCE COMPARISON

| Cases | Line | | | System | | Fault | | Z1 reach (pu) | Operating Time (ms) | | | |
|---|---|---|---|---|---|---|---|---|---|---|---|---|
| | V (kV) | Length (km) | L/R (ms) | SIR | L/R (ms) | Type | Location (pu) | | TD32 | PH32 | TD21 | PH21 |
| 1 | 230 | 159 | 25 | 0.13 | 19 | CAG | 0.18 | 0.85 | 2.3 | 7.6 | 2.8 | 9.6 |
| 2 | 230 | 159 | 25 | 0.18 | 37 | CAG | 0.82 | 0.85 | 2.0 | 13.9 | - | - |
| 3 | 230 | 159 | 25 | 0.13 | 19 | CG | 0.17 | 0.85 | 1.6 | 12.1 | 2.5 | 14.6 |
| 4 | 230 | 159 | 25 | 0.18 | 37 | CG | 0.83 | 0.85 | 3.0 | 20.6 | - | - |
| 5 | 230 | 56 | 29 | 0.33 | NA[1] | AG | 0.24 | 0.86 | 1.0 | 11.4 | 1.9 | 15.5 |
| 6 | 230 | 56 | 29 | 0.42 | NA[1] | CG | 0.53 | 0.86 | 1.1 | 14.1 | 6.9 | 20.4 |
| 7 | 230 | 56 | 29 | 0.33 | NA[1] | CG | 0.55 | 0.86 | 2.0 | 15.9 | 4.0 | 18.1 |
| 8 | 230 | 56 | 29 | 0.42 | NA[1] | CG | 0.52 | 0.86 | 1.1 | 14.9 | 2.6 | 17.2 |
| 9 | 161 | 117 | 16 | 0.09 | 10 | BG | 0.19 | 1.25 | 1.0 | 15.1 | - | 19.6 |
| 10 | 161 | 117 | 16 | ∞ | NA[2] | BG | 0.81 | 1.25 | 1.3 | 16.6 | - | 17.9 |
| 11 | 400 | 252 | 34 | 0.46 | 17 | AG | 0.14 | 0.80 | 1.6 | 14.4 | 3.4 | 14.4 |
| 12 | 400 | 252 | 34 | 0.46 | 27 | AG | 0.87 | 0.70 | 2.3 | 18.4 | - | - |
| 13 | 500 | 92 | 66 | 0.64 | NA[1] | BG | 0.01 | 0.76 | 1.0 | 12.1 | 2.6 | 18.5 |
| 14 | 500 | 92 | 66 | 0.32 | NA[1] | BG | 0.99 | 0.77 | 1.1 | 12.5 | - | - |

[1]Transients prevented us from calculating the system L/R ratio.
[2]Strong zero-sequence source prevented us from calculating the positive-sequence system L/R ratio.

assert. Fig. 16 plots the TD21 operating and restraining voltage to illustrate the TD21 security. The element has a considerable security margin.

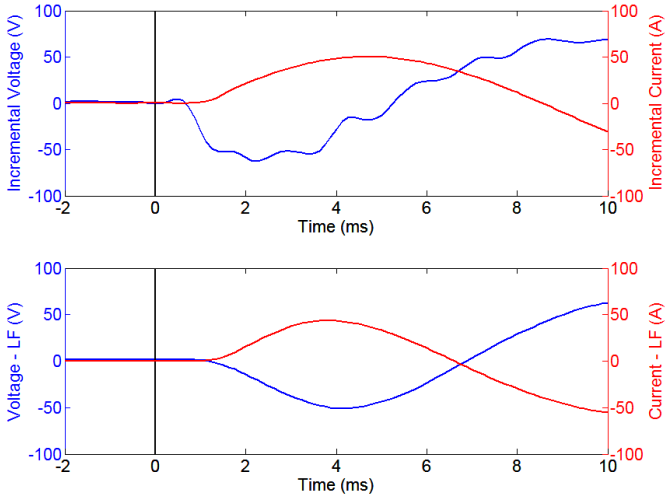


Fig. 13. Case 1: Loop incremental voltage ($\Delta v_{\Phi}$) and current ($\Delta i_{\Phi}$) for the faulted loop (top). Filtered loop incremental voltage ($\Delta v_{(LF)}$) and replica current ($\Delta i_{Z(LF)}$) for the TD21 element (bottom).

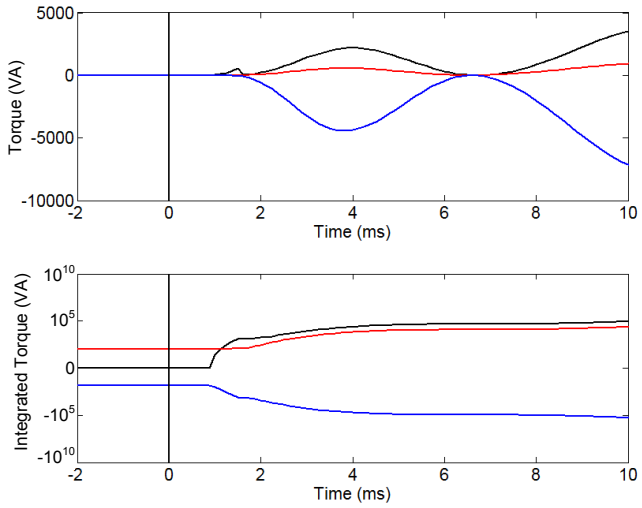


Fig. 14. Case 1: TD32 torques and integrated torques (operating: black, forward restraining: red, and reverse restraining: blue).

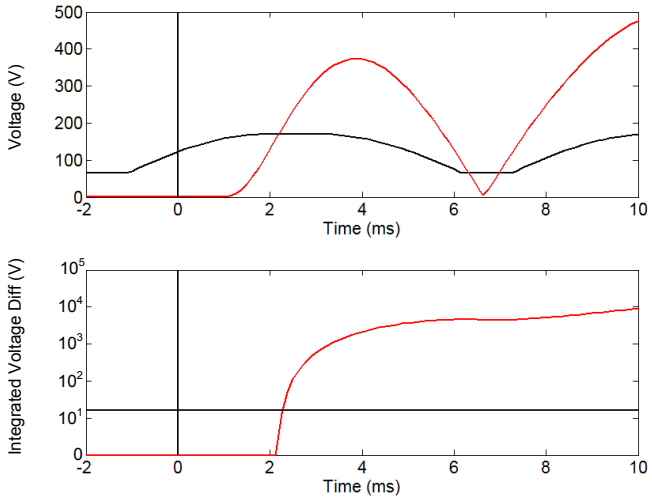


Fig. 15. Case 1: TD21 operating (red) and restraining (black) voltages (top), and the integrated voltage difference compared to a threshold (bottom).

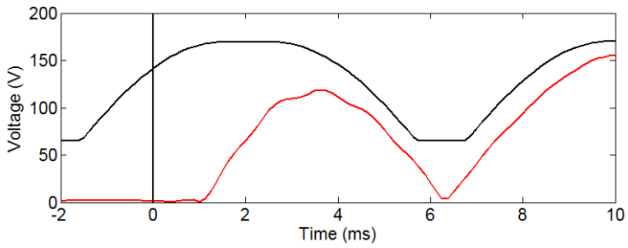


Fig. 16. Case 2: TD21 operating (red) and restraining (black) voltages. The fault is outside of the TD21 reach.

This case illustrated TD21 and TD32 operation for a very strong system. To evaluate the impact of the SIR, we plotted the operating time curves for a 100 km, 500 kV line with the SIR between 0.1 and 2. We assumed the same SIR for the positive- and zero-sequence networks. We simulated bolted faults for these tests using ten fault types and two points on wave (voltage zero and voltage peak). We modeled ideal instrument transformers in these tests.

Fig. 17 shows the average operating time of the TD21 element set to 80 percent of the line length. Fig. 18 shows the average operating time of the TD32 element.

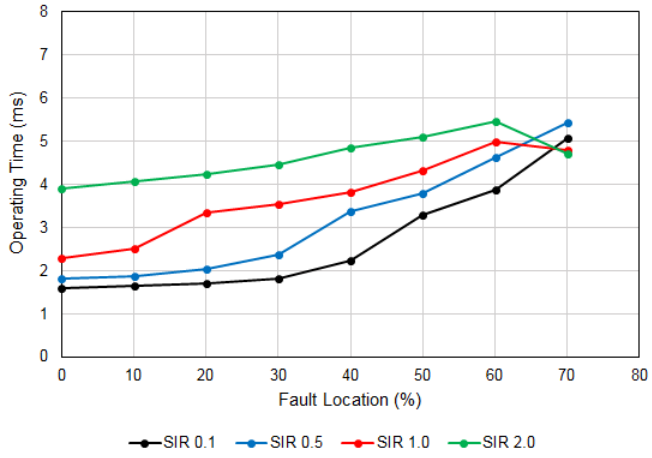


Fig. 17. TD21 element average operating time as a function of fault location for different values of the SIR.

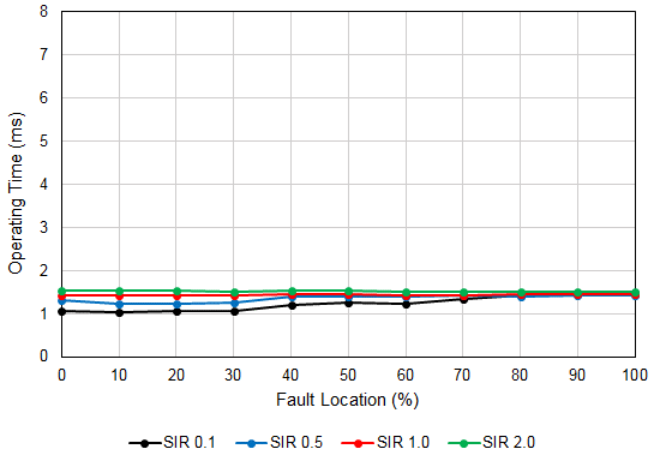


Fig. 18. TD32 element average operating time as a function of fault location for different values of the SIR.

The TD21 element operates on average below 2 ms for close-in faults in a strong system, as Case 1 illustrated. The TD21 element operates between 3 and 5 ms for the fault in the middle of the line depending on the SIR, and it operates in about 6 ms for faults very close to the reach point for relatively weak systems.

The TD21 element has good transient accuracy. We biased our TD21 design toward security. For relatively weak systems, the element does not respond to faults at the reach point. For strong systems, it shows less than 10 percent of overreach (when set to 80 percent of the line, it does not respond to faults at 90 percent of the line). The dependability of the element gradually decreases as the fault approaches the set reach point and as the system becomes weaker.

### *B. Case 6: Single-Line-to-Ground Fault on a Short Line*

A C-phase-to-ground (CG) fault near the middle of the line (0.53 pu) struck a 56 km, 230 kV line connected to a relatively strong system (SIR of 0.42). The in-service relay asserted its forward directional element in 14.1 ms and tripped from distance Zone 1 in 20.4 ms. The TD32 and TD21 elements responded in 1.1 ms and 6.9 ms, respectively (Fig. 19).

Fig. 20 shows the loop voltage and current. In this case, the incremental replica current starts with negative polarity but changes polarity to positive before reaching its full fault magnitude (effect of the point on wave). This pattern does not affect the TD32 element, which operates reliably and fast. It affects the speed of the TD21 element, however. As shown in Fig. 21, the TD21 operating voltage is close to the restraining voltage at 3 ms into the fault, but it exceeds the restraining voltage at about 6 ms (when the current changed polarity and developed higher in the positive direction). This case illustrates how the point on wave impacts the TD21 element response.

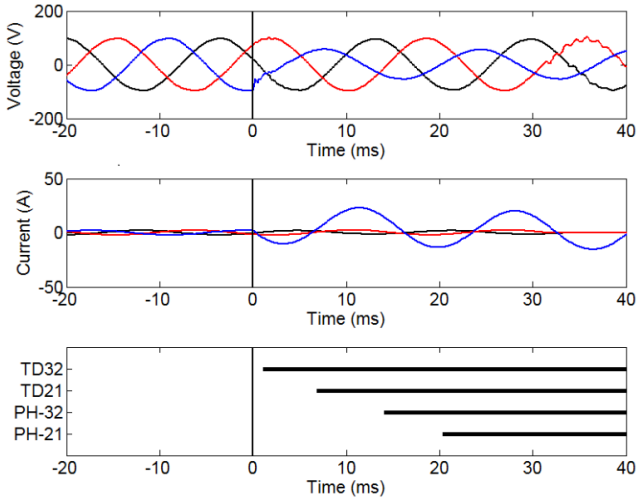


Fig. 19. Case 6: Relay voltage and current and the outputs of the directional and underreaching elements.

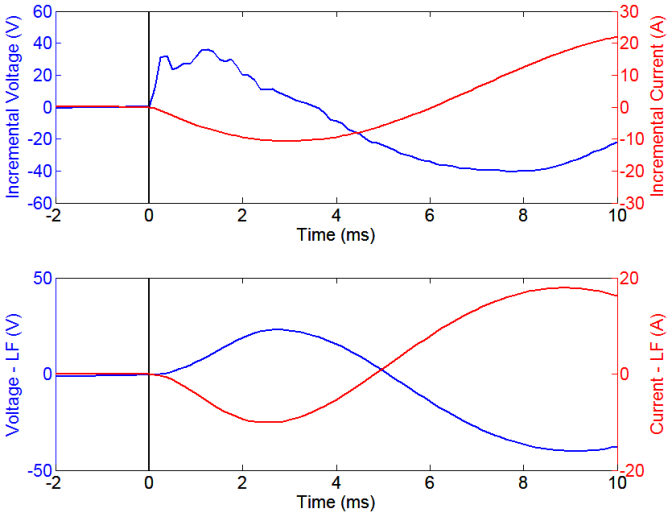


Fig. 20. Case 6: Loop incremental voltage and current for the faulted loop (top). Filtered loop incremental voltage and replica current for the TD21 element (bottom).

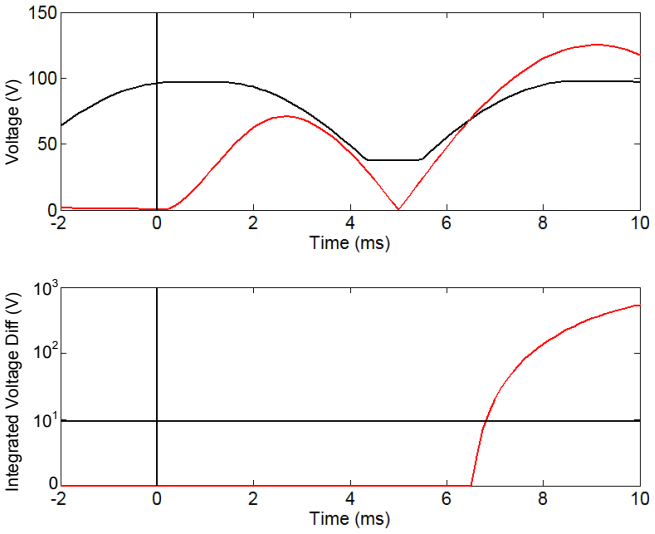


Fig. 21. Case 6: TD21 operating (red) and restraining (black) voltages (top), and the integrated voltage difference compared to a threshold (bottom).

To better explain how the point on wave impacts the operating time of the TD21 and TD32 elements, we used a 100 km line with an SIR of 1 and simulated faults at 30 percent of the line (the TD21 reach is set to 80 percent). We initiated faults at various loop voltage levels from –1 pu (negative peak) to +1 pu (positive peak) in increments of 0.2 pu and recorded the TD21 and TD32 operating times. Fig. 22 presents the results for the single-line-to-ground (SLG) faults.

Varying the point on wave causes approximately 1.5 ms variability in the TD32 operating time and about 3 ms variability in the TD21 operating time. The elements operate the fastest for faults near the voltage peak. This is because the source in the incremental-quantity circuit has the highest magnitude when the fault causes the voltage to drop from the maximum value.

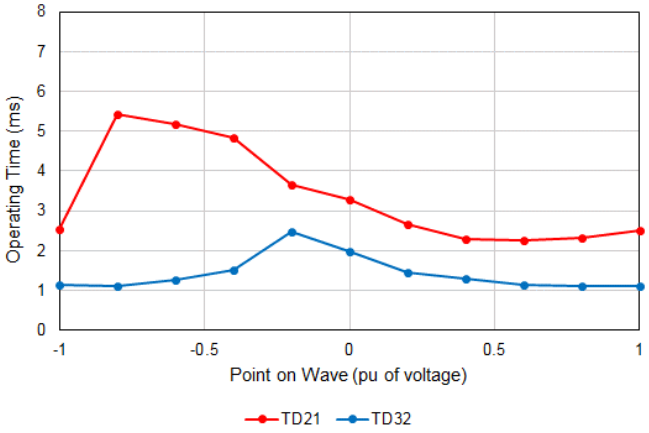


Fig. 22. Impact of the point on wave on the operating time of the TD21 and TD32 elements for SLG faults.

### C. *Case 10: Single-Line-to-Ground Fault With Weak Feed*

A B-phase-to-ground (BG) fault at 0.81 pu struck a 117 km, 161 kV line connected to a ground source (transformer grounded-wye winding). There is no positive-sequence source at this terminal. The zero-sequence SIR is about 0.36. The in-service relay asserted the Zone 1 element (configured as an overreaching element) in 17.9 ms and its forward directional element in 16.6 ms. The TD32 element responded in 1.3 ms, and the TD21 element did not respond to this fault (Fig. 23).

In this case, the faulted phase voltage collapsed dramatically (no positive- or negative-sequence current feed from this terminal) and the fault current has only a zero-sequence component (with only the ground source present behind the relay, all three currents are equal and in phase as shown in Fig. 23).

Despite the absence of a positive-sequence source behind the relay, the incremental voltage and current are significant (Fig. 24). As a matter of fact, the weaker the system, the larger the incremental voltage. In this case, however, the system $Z_0/Z_1$ ratio is dramatically different than the line $Z_0/Z_1$ ratio used in calculating the replica current. This difference is responsible for the slightly different shape of the incremental voltage and the loop replica current (Fig. 24). Despite this inaccuracy, the two signals, when processed by the TD32 logic, clearly indicate a forward fault and allow the TD32 element to operate reliably and fast (Fig. 25).

Fig. 26 shows the operating and retraining voltages of the TD21 element. The operating signal is only marginally higher than the restraining signal because the fault is practically at the reach point of the TD21 element. The element would have operated at about 9 ms into the fault, but the security window had already expired.

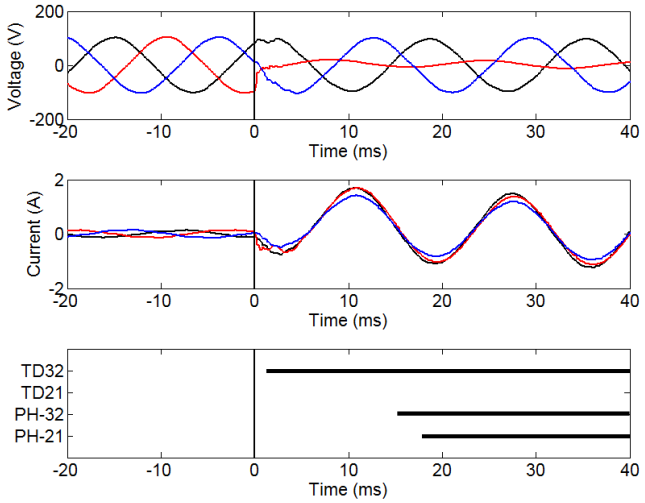


Fig. 23. Case 10: Relay voltage and current and the outputs of the directional and underreaching elements.

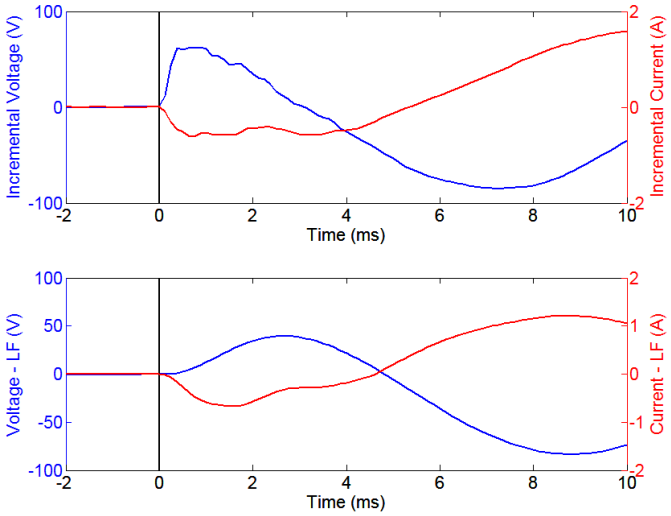


Fig. 24. Case 10: Loop incremental voltage and current for the faulted loop (top). Filtered loop incremental voltage and replica current for the TD21 element (bottom).

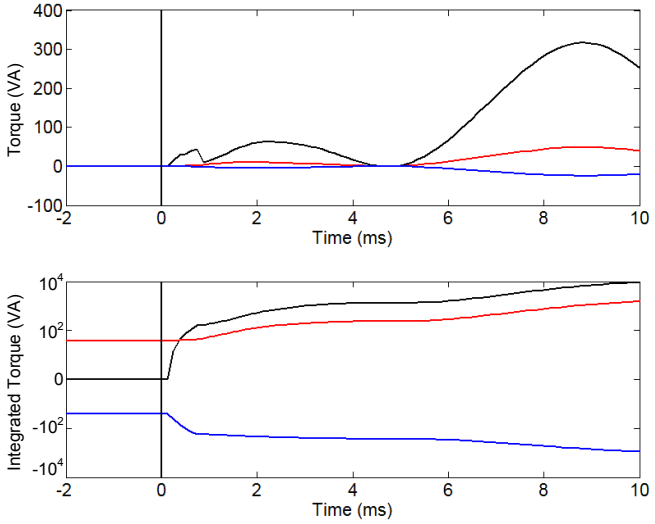


Fig. 25. Case 10: TD32 torques and integrated torques (operating: black, forward restraining: red, and reverse restraining: blue).

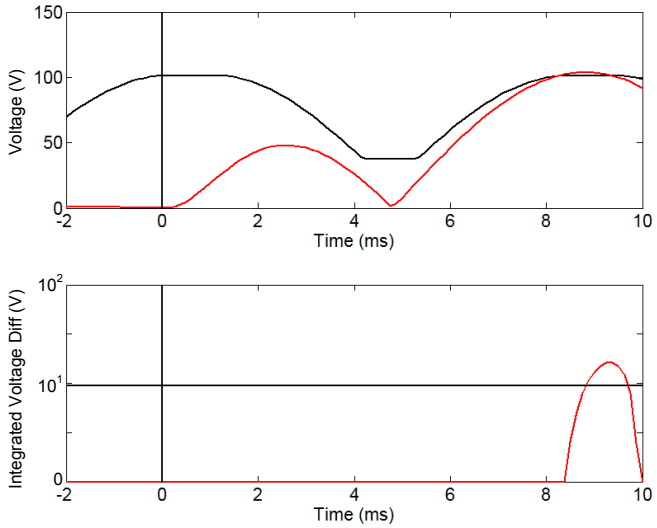


Fig. 26. Case 10: TD21 operating (red) and restraining (black) voltages (top), and the integrated voltage difference compared to a threshold (bottom).

### *D. Case 11: Single-Line-to-Ground Fault on a Long Line*

An A-phase-to-ground (AG) close-in (0.14 pu) fault struck a 252 km, 400 kV line connected to a relatively strong system (SIR of 0.46). The in-service relay asserted its forward directional element in 14.4 ms and tripped from distance Zone 1 in 14.4 ms. The TD32 and TD21 elements responded in 1.6 ms and 3.4 ms, respectively (Fig. 27). Fig. 28 illustrates the operation of the TD32 element.

Fig. 29 illustrates the response of the TD21 element. The element operated quickly, despite the replica current developing relatively slowly. Had the element missed the opportunity to trip in 3 ms, it would have operated in about 5 ms.

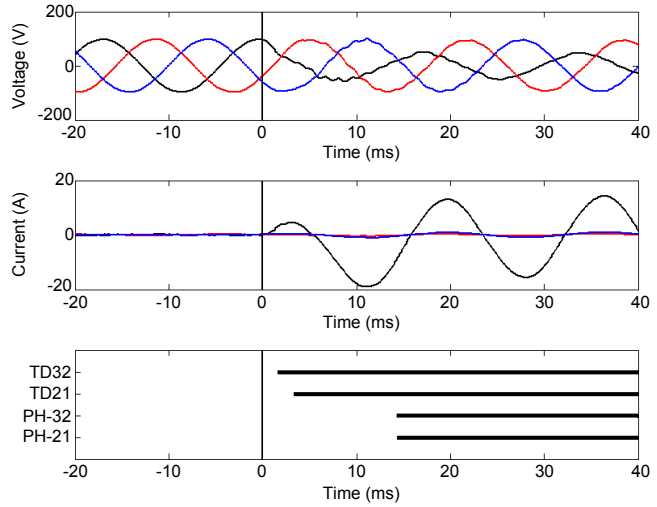


Fig. 27. Case 11: Relay voltage and current and the outputs of the directional and underreaching elements.

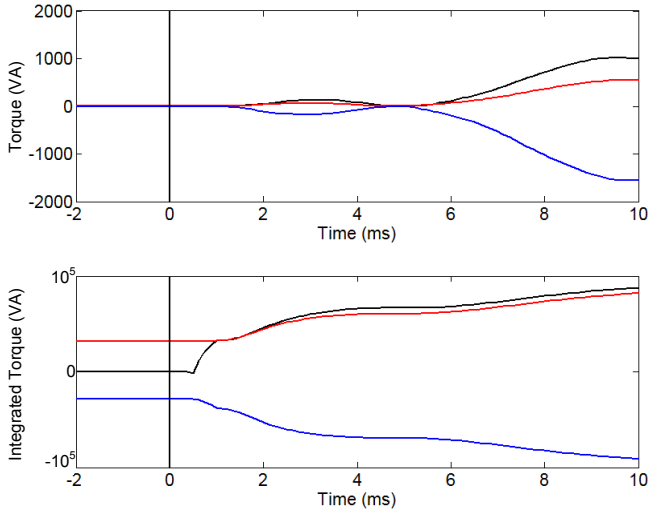


Fig. 28. Case 11: TD32 torques and integrated torques (operating: black, forward restraining: red, and reverse restraining: blue).

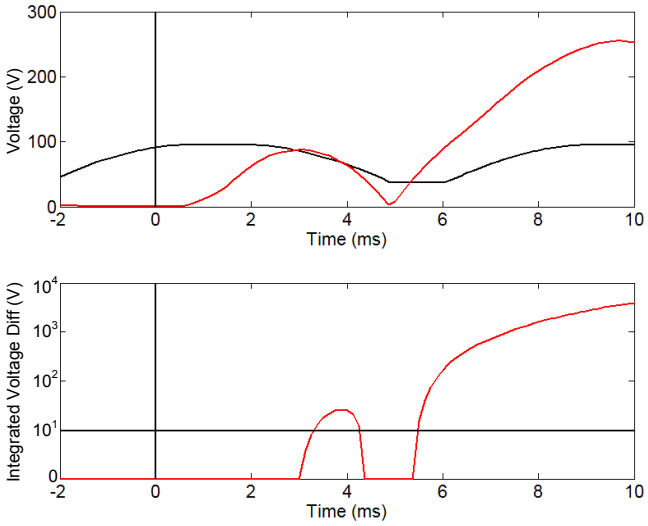


Fig. 29. Case 11: TD21 operating (red) and restraining (black) voltages (top) and the integrated voltage difference compared to a threshold (bottom).

### *E. Case 12: Remote Relay in Case 11*

This case refers to the remote terminal of Case 11. This terminal also operates at a relatively low SIR (0.46). The fault is located at 0.86 pu, i.e., 6 percent beyond the TD21 reach point. Fig. 30 shows the relay voltages and currents and the responses of the elements.

Fig. 31 shows the operating and restraining voltages of the TD21 element. The operating signal is considerably below the restraining signal, providing the TD21 element with good security margin. Given the fault location (6 percent beyond the TD21 reach point), this security margin is larger than expected. The CCVT transient is responsible for the difference. Initially, the CCVT secondary voltage is larger than the ratio voltage (the CCVT secondary voltage is overestimated). As a result, the incremental secondary voltage is initially underestimated. This, in turn, leads to the TD21 element underreaching due to the CCVT transient rather than overreaching. Later during the fault, the CCVT transient can lead to the underestimation of the secondary voltage and overestimation of the secondary

incremental voltage. This situation may lead to overreaching. Our TD21 design intentionally inhibits the element before the incremental voltage overshoots as a result of the CCVT transient. An important observation is that unlike the case of phasor-based protection, the CCVT transient improves the TD21 element security (and may slow it down to a certain degree).

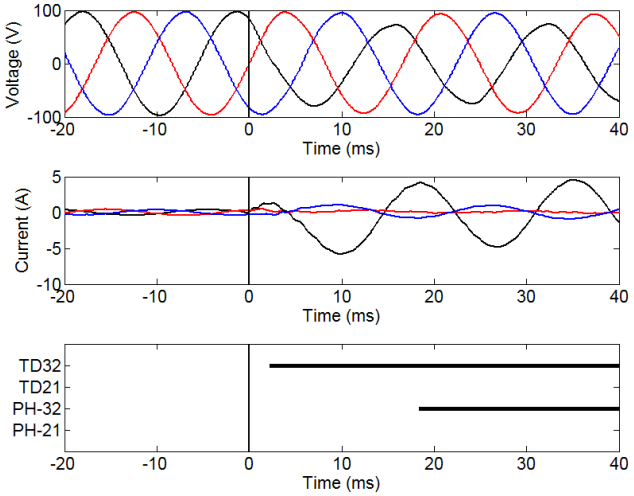


Fig. 30. Case 12: Relay voltage and current and the outputs of the directional and underreaching elements.

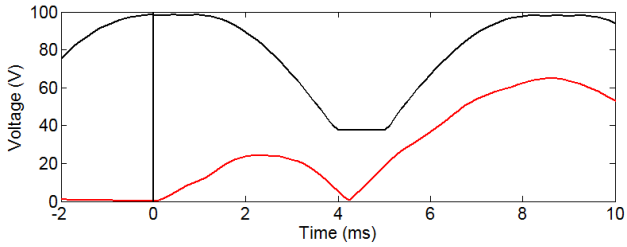


Fig. 31. Case 13: TD21 operating (red) and restraining (black) voltages.

Cases 11 and 12 have been captured on a relatively long line. Longer lines draw more charging current. A large charging current violates the RL line model used to derive the TD21 and TD32 principles. Therefore, it is important to consider lines of various lengths in the element design and testing. The TD32 element has considerable margin and performs very well for different line lengths.

Our design applies more conservative TD21 filtering for long lines in order to better dampen transients in the TD21 operating signal. These transients result from the line shunt capacitance and have lower frequencies as the line lengthens. Fig. 32 shows the minimum and average operating times for the TD21 element for several line lengths. We simulated ten bolted fault types and two points on wave (voltage zero and voltage peak), for an SIR of 0.1.

We observe that the operating times for short and medium-length lines are similar. The operating time for long lines is slightly slower because of the extra group delay caused by lowering the cut-off frequency of the TD21 low-pass filter. Nonetheless, for strong systems, the element responds as fast as 2 ms to 4 ms on average for faults closer than 50 percent of the line.

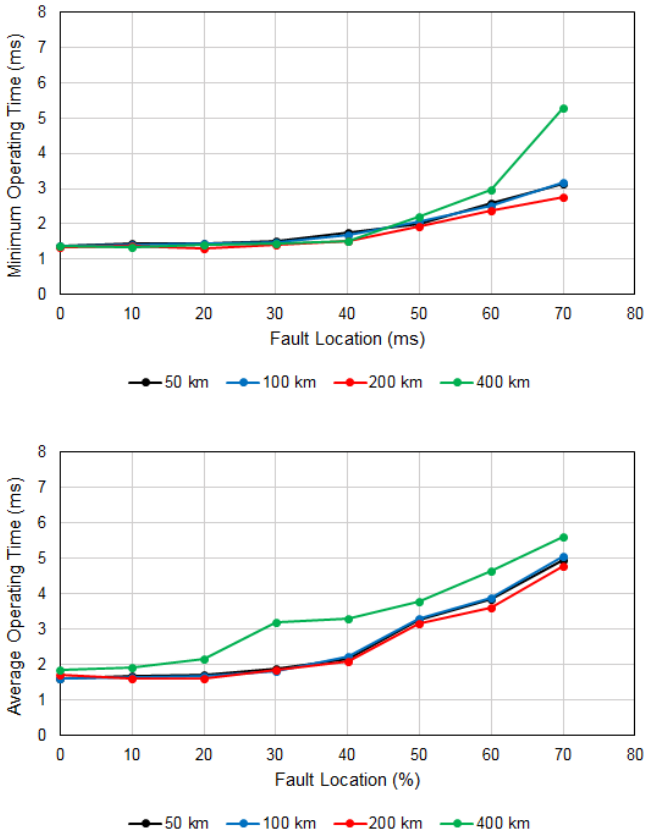


Fig. 32. TD21 element minimum and average operating time as a function of fault location for different line lengths.

### *F. Case 13: Single-Line-to-Ground Fault on Series-Compensated Line*

A B-phase-to-ground (BG) close-in (0.01 pu) fault struck a 92 km, 500 kV series-compensated line connected to a relatively strong system (SIR of 0.64). The in-line series compensation level is 75 percent. The capacitors are located at the line end, and line-side VTs are used for line protection. The adjacent lines are series compensated as well. The in-service relay asserted its forward directional element in 12.1 ms and tripped from distance Zone 1 in 18.5 ms. The TD32 and TD21 elements responded in 1.0 ms and 2.6 ms, respectively (Fig. 33).

Fig. 34 shows the incremental voltage and current for the BG loop. Despite series compensation, the incremental voltage and the incremental replica current are of opposite polarities except for the brief period between about 5 and 7 ms. The integrated torque, however, rides very well through this period, and the TD32 element operates quickly and with excellent security and dependability margins (Fig. 35).

Fig. 36 shows the TD21 operating and restraining voltage. In applications with series compensation on adjacent lines, it is impossible to calculate the TD21 restraining voltage using the approach outlined in Section II. Therefore, our TD21 design assumes the worst-case TD21 restraint (the nominal voltage plus margin), instead of using the point-on-wave restraint as in the case of noncompensated lines. Despite this conservative restraint, the TD21 element operates reliably and as quickly as expected for a close-in fault in a strong system.

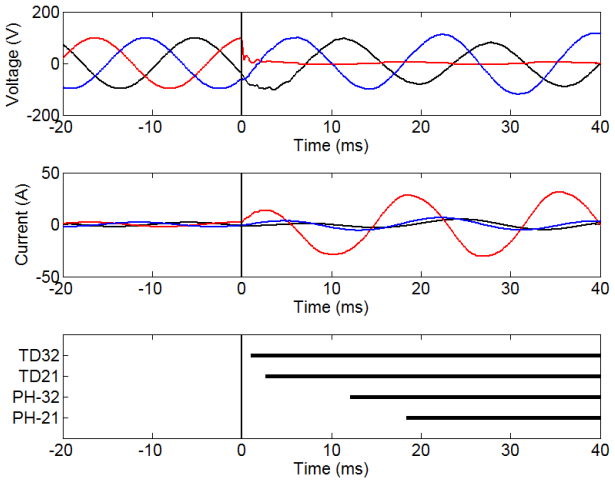


Fig. 33. Case 13: Relay voltage and current and the outputs of the directional and underreaching elements.

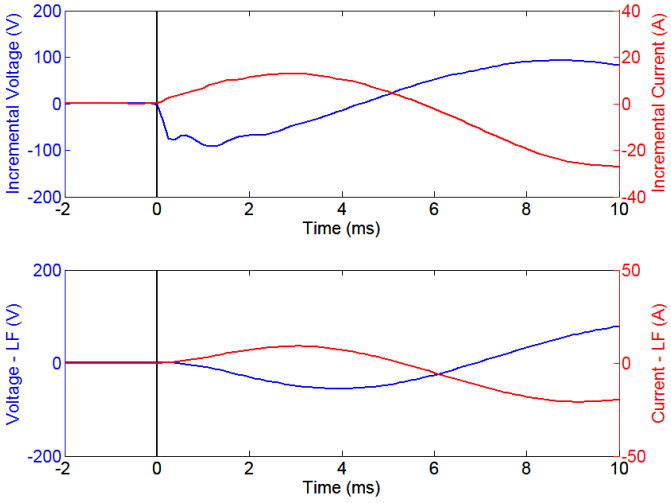


Fig. 34. Case 13: Unfiltered incremental loop voltage and current for the faulted loop (top). Filtered incremental voltage and replica current for TD21 element (bottom).

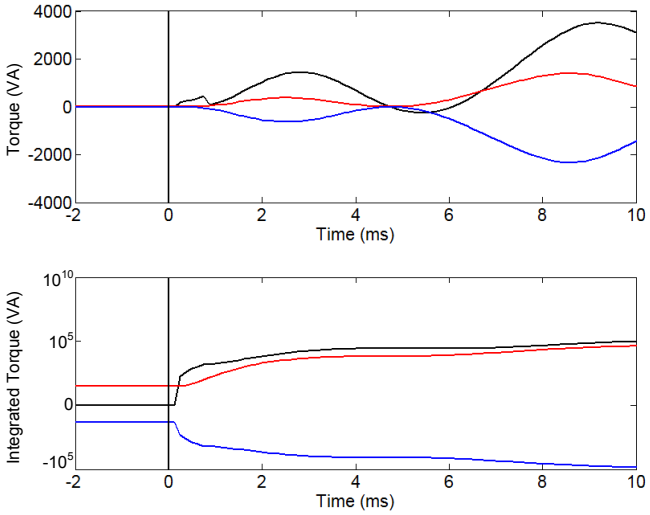


Fig. 35. Case 13: TD32 torques and integrated torques (operating: black, forward restraining: red, and reverse restraining: blue).

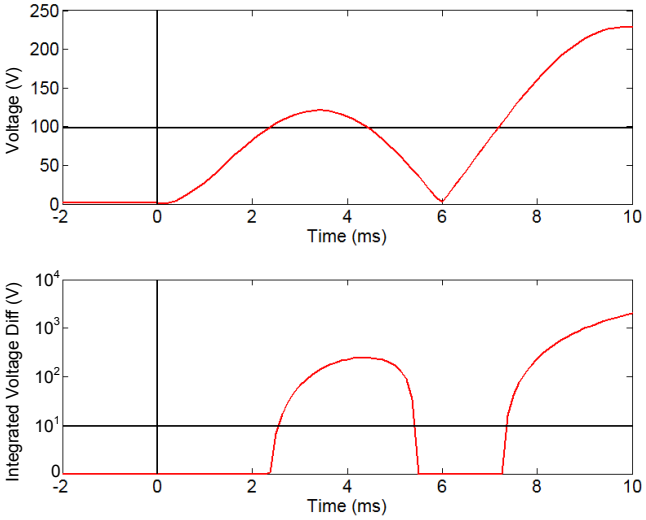


Fig. 36. Case 13: TD21 operating (red) and restraining (black) voltages (top), and the integrated voltage difference compared to a threshold (bottom).

## IV. Performance on TW-Based Line Protection

In this section, we illustrate performance of TW-based line protection using both digital simulations and a selected field case.

### *A. TW32 and TW87 Examples Using EMTP-Simulated Cases*

We used an electromagnetic transient program (EMTP) to simulate an AG fault at three different locations in a simple 500 kV system as shown in Fig. 37. The fault resistance is zero, and the fault occurs at the voltage peak. The line length is 161 km, and the TW propagation time is 542 μs. We simulated ideal CTs and VTs with 600:1 and 4500:1 ratios, respectively.

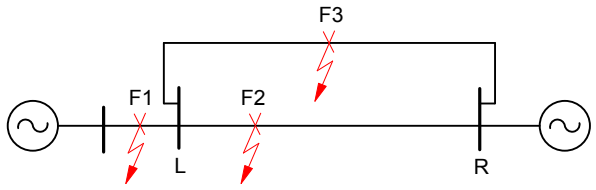


Fig. 37. Simple system for illustrating the TW32 and TW87 principles.

#### *1) Close-In External Fault (F1)*

Fig. 38 shows currents and voltages for external fault F1 and the TW differential and directional outputs. Fig. 39 shows the current TWs at the local and remote terminals. As expected, the TWs measured at the L terminal with negative polarity (Phase A) are measured at the R terminal with positive polarity exactly 542 μs later. We see the same pattern in all three phases. Table II lists the signals calculated from the measured TWs and used by the TW87 logic.

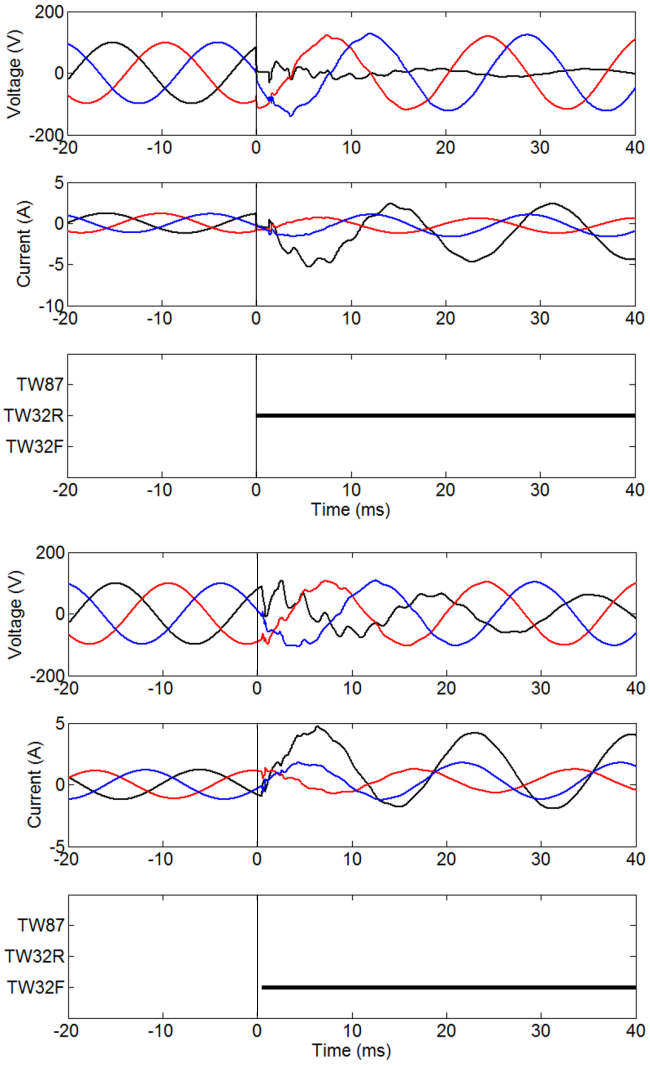


Fig. 38. Local (top) and remote (bottom) voltages and currents, and the TW differential and directional outputs for the external fault F1.

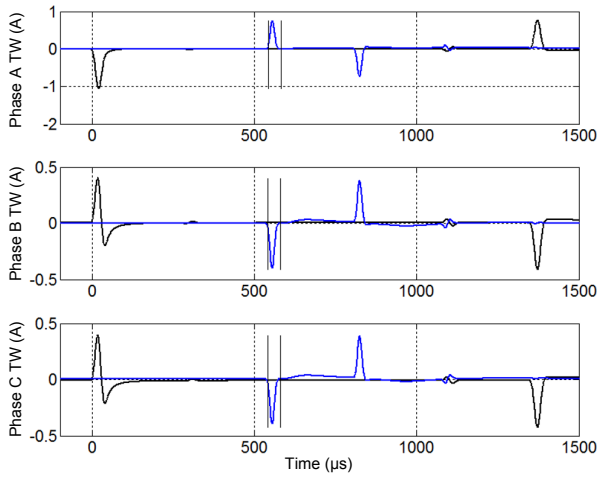


Fig. 39. Local (black) and remote (blue) current TWs for the external fault F1.

For the external fault F1, the TW87 algorithm calculates the operating signal well below the restraining signal (0.66 A vs. 2.16 A in Phase A, for example) and the element restrains with a large security margin.

Fig. 40 presents the A-phase voltage and current TWs at the local terminal and the integrated TW32 torque. The torque is decisively negative, and the TW32 element indicates a reverse fault direction.

TABLE II
TW87 SIGNALS FOR THE EMTP EXAMPLES

| Fault | Φ | $I_L$ (A) | $I_R$ (A) | $I_{DIF}$ (A) | $I_{RST}$ (A) | $m_{87}$ (pu) |
|---|---|---|---|---|---|---|
| F1 | A | 1.41 | 0.75 | 0.66 | 2.16 | 1.0 |
| | B | 0.40 | 0.40 | 0.01 | 0.80 | 1.0 |
| | C | 0.38 | 0.38 | 0.00 | 0.76 | 1.0 |
| F2 | A | 1.22 | 0.76 | 1.98 | 1.22 | 0.4 |
| | B | 0.51 | 0.39 | 0.90 | 0.51 | 0.4 |
| | C | 0.54 | 0.38 | 0.92 | 0.54 | 0.4 |
| F3 | A | 0.92 | 0.53 | 1.45 | 1.70 | 0.3 |
| | B | 0.31 | 0.27 | 0.58 | 0.74 | 0.3 |
| | C | 0.30 | 0.28 | 0.57 | 0.72 | 0.3 |

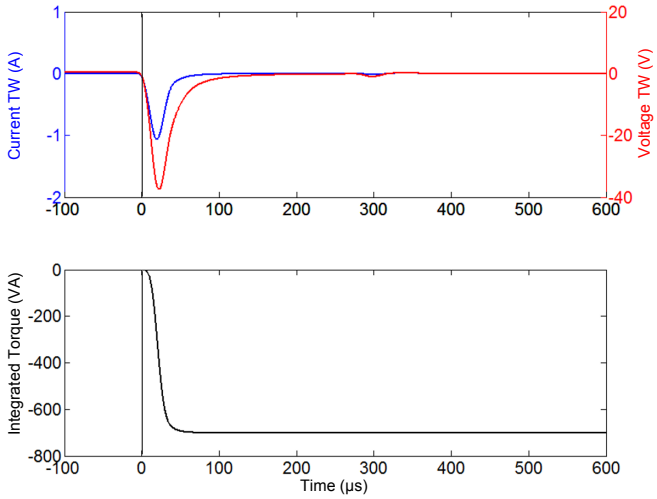


Fig. 40. Voltage and current TWs and the integrated TW32 torque at the local terminal for the external fault F1.

*2) Internal Fault (F2)*

Fig. 41 shows currents and voltages for internal fault F2 at 0.4 pu from the local terminal along with the TW differential and directional outputs. Fig. 42 plots the TW87 currents, and Fig. 43 plots the TW32 quantities at the local terminal. Table II lists the signals calculated from the measured TWs and used by the TW87 logic.

The TW87 element calculates the fault location as about 0.4 pu, and there is a very good agreement among calculations in all three phases. The TW87 operating signal is considerably above the restraining signal (1.98 A vs. 1.22 A in Phase A, for example), and the element operates dependably.

The TW32 element measures a decisively positive torque (Fig. 43) and indicates a forward fault direction dependably. Note that the second TW measured at around 280 μs is a reverse wave, a reflection from behind the relay. This wave reduces the

integrated torque but does not reverse its polarity because each reflection has a lower magnitude than the original TW.

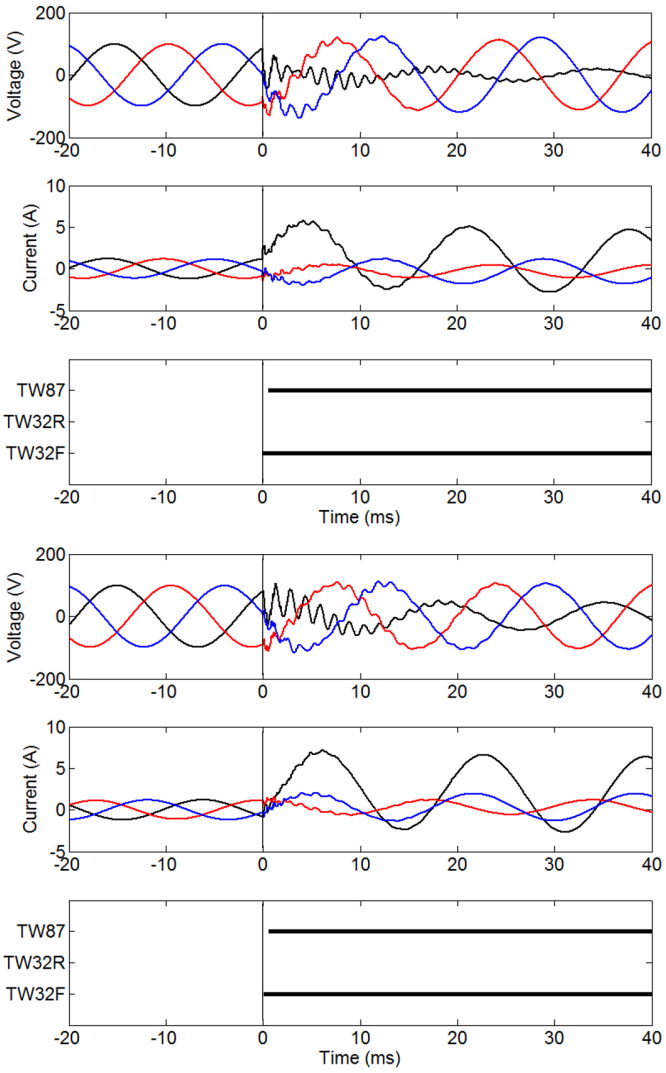


Fig. 41. Local (top) and remote (bottom) voltages and currents, and the TW differential and directional outputs for the internal fault F2.

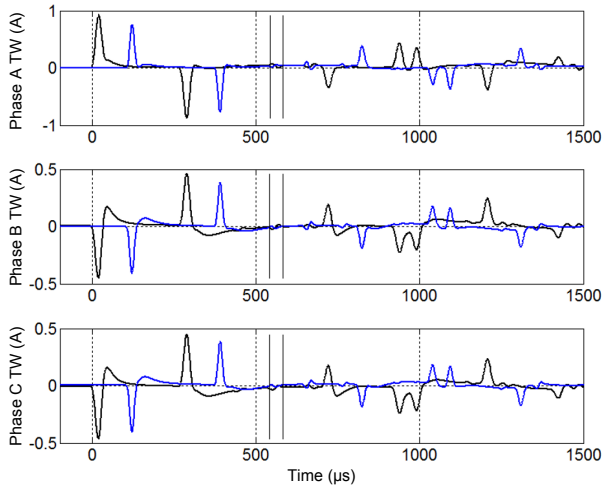


Fig. 42. Local (black) and remote (blue) current TWs for the internal fault F2.

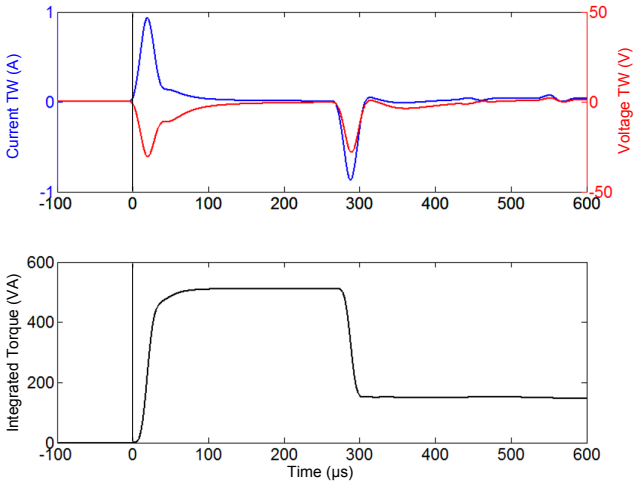


Fig. 43. Voltage and current TWs and the integrated TW32 torque at the local terminal for the internal fault F2.

*3) External Fault (F3)*

Fig. 44 shows voltages and currents for an external fault located in such a way that the TWs reached the local and remote terminals at approximately the same time (the difference is less than the line propagation time) and with the same polarity. Table II lists the signals calculated from the measured TWs and used by the TW87 logic.

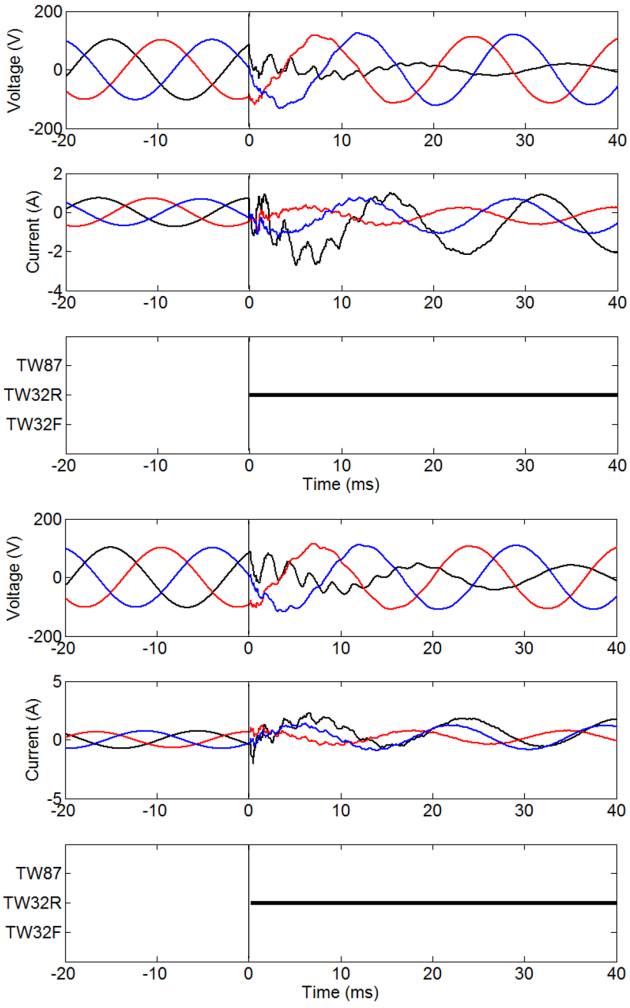


Fig. 44. Local (top) and remote (bottom) voltages and currents for the external fault F3.

Fig. 45 shows the local and remote current TWs. The TW87 element calculates the fault location as 0.3 pu. Considering the polarities and the time difference between the first TWs recorded at each line terminal, the fault appears to be internal, located 0.3 pu from the local terminal. However, the TW87 element inspects the TWs one line propagation time past the initial waves and sees the TWs with the opposite polarity as they leave the protected line. As a result, the operating signal is lower than the restraining signal (1.45 A vs. 1.70 A in Phase A, for example), and the TW87 element restrains with a good margin.

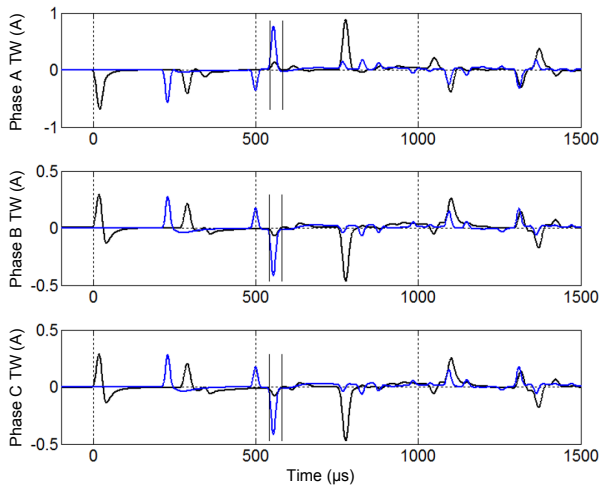


Fig. 45. Local (black) and remote (blue) current TWs for external fault F3.

### B. TW87 Example Using Field Data

We have captured time-synchronized current TWs for Cases 9 and 10 in Table I. The fault was located at 0.81 pu from the local terminal, and the line propagation time is 396 μs. These TWs have been captured and measured using the circuitry developed for the fault-locating function [2]. Nonetheless, we can use them to illustrate the TW87 principle and implementation. Fig. 46 shows the local and remote current TWs, and Table III lists the calculated TW87 signals. These values appear low for a 5A nominal relay. The current TWs are actually higher and the difference results from the specific hardware gain of the fault locator that captured the record.

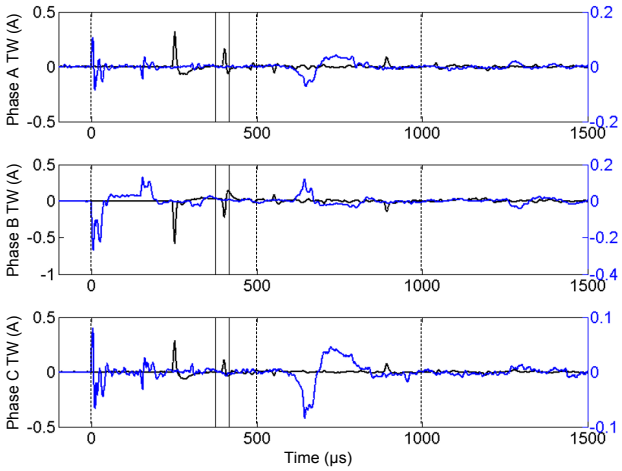


Fig. 46. Local (black) and remote (blue) current TWs captured for Cases 10 and 11.

TABLE III
TW87 SIGNALS FOR FIELD CASES 10 AND 11

| Φ | IL (A) | IR (A) | $I_{DIF}$ (A) | $I_{RST}$ (A) | $m_{87}$ (pu) |
|---|---|---|---|---|---|
| A | 0.38 | 0.06 | 0.44 | 0.12 | 0.799 |
| B | 0.68 | 0.35 | 1.03 | 0.13 | 0.811 |
| C | 0.34 | 0.04 | 0.38 | 0.07 | 0.798 |

The TW87 algorithm verifies the fault location correctly (0.798–0.811 pu calculated by $m_{87}$ in real time vs. 0.81 pu from the TW fault locator) and operates dependably for this fault because the operating signal in the B-phase is considerably higher than the restraining signal (1.03 A vs. 0.13 A).

## V. COMPARATIVE RELAY TESTING

In Section III, we compared the incremental-quantity-based elements with the in-service relays for a handful of field cases. In this section, we apply a large number of simulated fault cases to obtain a more rigorous comparison between time-domain and phasor-based relays.

We tested the TD21 and TD32 elements against the Zone 1 and directional elements, respectively, of two high-performance, phasor-based line protection relays A and B. We set the underreaching elements to 80 percent of the line length. All relays use solid-state trip-rated outputs.

We modeled a 161 km, 500 kV line with SIR of 1.4 at both terminals. We simulated bolted faults for these tests using ten fault types and two points on wave (voltage zero and voltage peak). We modeled ideal instrument transformers in these tests.

Fig. 47 presents the operating times for the TD21 and Zone 1 elements in relays A and B. Relays A and B operate in less than a cycle for close-in faults. Relay A is a one-cycle relay for midline faults, while Relay B takes 1.5 cycles to operate for midline faults. Their operating times for faults close to the reach point are in the order of 2 cycles for the test conditions that we applied. Both relays A and B exhibit a relatively large spread in their operating times. The TD21 element, in turn, is consistently fast with the average operating time below 4 ms.

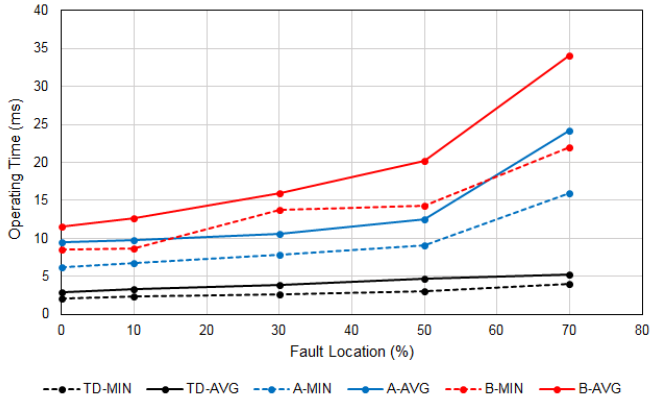


Fig. 47. Operating times of the tested underreaching elements.

Fig. 48 presents the distribution function of the difference in the operating times between the TD21 and Relay A for faults up to the midpoint of the line. In all cases, the TD21 is faster:

on average by about 7 ms, sometimes by as much as 11 ms, and sometimes by only 2 ms.

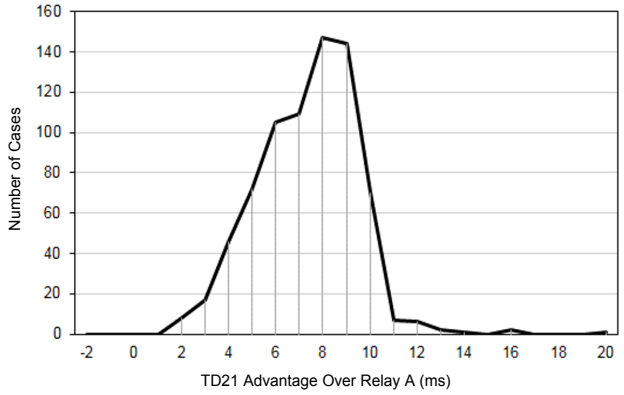


Fig. 48. Distribution of the difference between the operating times of TD21 and Relay A.

Fig. 49 presents the operating times for the overreaching directional elements. Relay A operates in about half a cycle. Relay B takes 1 to 1.5 cycles to detect the fault direction. The TD32 element operates consistently in about 2 ms.

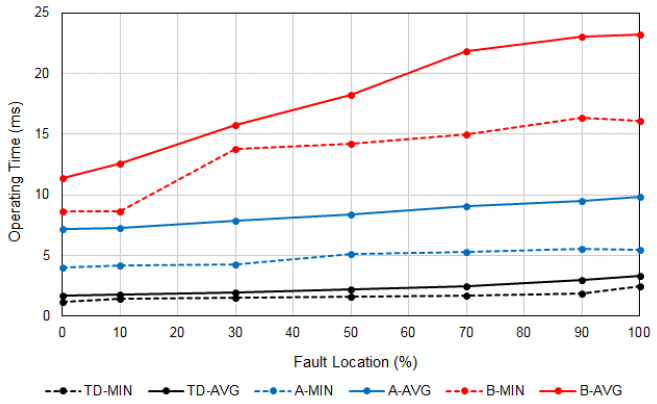


Fig. 49. Operating times of the tested directional elements.

## VI. Conclusions

We explained the operating principles of time-domain line protection elements: incremental-quantity directional and distance, and TW line current differential and directional. We also shared some key implementation details for better understanding and independent verification of the protection elements. These elements are implemented using high-speed sampling and simple operations including filtering, integration, comparison, timers, and logic gates. As such, the new principles are easy to understand and simple to apply.

We used a number of real-world line faults to illustrate the operation of the time-domain line protection elements and show the difference in performance compared with traditional phasor-based protection. The field cases demonstrate dependability and speed improvements. They also demonstrate security of the time-domain elements. Each remote-end line fault is a security test for our underreaching element, and each forward fault is a security test for our reverse-looking directional element. The tested elements operated for all line faults within their intended reach, with operating times faster by 6 to 20 ms as compared with the in-service phasor-based relays.

We evaluated the time-domain elements with respect to a number of factors that affect line protection performance—including fault location, system strength, and point on wave—while using two different phasor-based relays for comparison. Our testing shows the operating times for our time-domain line protection elements are in the order of 2 ms for the TD32, 1 ms for the TW32, 4 ms for the TD21, and less than 1 ms plus the channel time for the TW87.

We intentionally biased the time-domain elements for speed and security instead of perfect dependability. Therefore, they require dependable, typically phasor-based, protection elements operating in parallel either as a part of the same relay, or as a separate relay. However, these fast elements operate for a large percentage of line faults. As a result, the dependable but slower backup is called upon infrequently, resulting in excellent average operating times of the complete application.

## VII. References

[1] E. O. Schweitzer, III, B. Kasztenny, A. Guzmán, V. Skendzic, and M. V. Mynam, "Speed of Line Protection – Can We Break Free of Phasor Limitations?" proceedings of the 41st Annual Western Protective Relay Conference, Spokane, WA, October 2014.

[2] E. O. Schweitzer, III, A. Guzmán, M. V. Mynam, V. Skendzic, B. Kasztenny, and S. Marx, "Locating Faults by the Traveling Waves They Launch," proceedings of the 40th Annual Western Protective Relay Conference, Spokane, WA, October 2013.

[3] M. Ando, E. O. Schweitzer, III, and R. A. Baker, "Development and Field-Data Evaluation of Single-End Fault Locator for Two-Terminal HVDC Transmission Lines, Part I: Data Collection System and Field Data," *IEEE Transactions on Power Apparatus and Systems*, Vol. PAS–104, Issue 12, December 1985, pp. 3524–3530.

[4] M. Ando, E. O. Schweitzer, III, and R. A. Baker, "Development and Field-Data Evaluation of Single-End Fault Locator for Two-Terminal HVDC Transmission Lines, Part II: Algorithm and Evaluation," *IEEE Transactions on Power Apparatus and Systems*, Vol. PAS–104, Issue 12, December 1985, pp. 3531–3537.

[5] A. T. Johns, "New Ultra-High-Speed Directional Comparison Technique for the Protection of EHV Transmission Lines," *IEE Proceedings C: Generation, Transmission, and Distribution*, Vol. 127, Issue 4, July 1980, pp. 228–239.

[6] T. Takagi, J. Barbar, U. Katsuhiko, and T. Sakaguchi, "Fault Protection Based on Travelling Wave Theory, Part I: Theory," *IEEE Power Engineering Society Summer Meeting*, Mexico, Paper A77, July 1977, pp. 750–753.

[7] H. W. Dommel and J. M. Michels, "High Speed Relaying Using Traveling Wave Transient Analysis," IEEE Power Engineering Society Winter Meeting, New York, Paper No. A78, January/February 1978, pp. 214–219.

[8] K. Zimmerman and D. Costello, "Fundamentals and Improvements for Directional Relays," proceedings of the 63rd Annual Conference for Protective Relay Engineers, College Station, TX, March/April 2010.

[9] M. Vitins, "A Fundamental Concept for High Speed Relaying," *IEEE Transactions on Power Apparatus and Systems*, Vol. PAS–100, Issue 1, January 1981, pp. 163–173.

## VIII. Biographies

**Dr. Edmund O. Schweitzer, III** is recognized as a pioneer in digital protection and holds the grade of Fellow in the IEEE, a title bestowed on less than one percent of IEEE members. In 2002, he was elected as a member of the National Academy of Engineering. Dr. Schweitzer received the 2012 Medal in Power Engineering, the highest award given by IEEE, for his leadership in revolutionizing the performance of electrical power systems with computer-

based protection and control equipment. Dr. Schweitzer is the recipient of the Regents' Distinguished Alumnus Award and Graduate Alumni Achievement Award from Washington State University and the Purdue University Outstanding Electrical and Computer Engineer Award. He has also been awarded honorary doctorates from both the Universidad Autónoma de Nuevo León, in Monterrey, Mexico, and the Universidad Autónoma de San Luis Potosí, in San Luis Potosí, Mexico, for his contributions to the development of electric power systems worldwide. He has written dozens of technical papers in the areas of digital relay design and reliability, and holds nearly 200 patents worldwide pertaining to electric power system protection, metering, monitoring, and control. Dr. Schweitzer received his bachelor's and master's degrees in electrical engineering from Purdue University, and his doctorate from Washington State University. He served on the electrical engineering faculties of Ohio University and Washington State University, and in 1982, he founded Schweitzer Engineering Laboratories, Inc. to develop and manufacture digital protective relays and related products and services.

**Bogdan Kasztenny** is the R&D director of protection technology at Schweitzer Engineering Laboratories, Inc. He has over 25 years of expertise in power system protection and control, including 10 years of academic career and 15 years of industrial experience, developing, promoting, and supporting many protection and control products. Bogdan is an IEEE Fellow, Senior Fulbright Fellow, Canadian representative of CIGRE Study Committee B5, registered professional engineer in the province of Ontario, and an adjunct professor at the University of Western Ontario. Since 2011, Bogdan has served on the Western Protective Relay Conference Program Committee. Bogdan has authored about 200 technical papers and holds 30 patents.

**Mangapathirao (Venkat) Mynam** received his MSEE from the University of Idaho in 2003 and his BE in electrical and electronics engineering from Andhra University College of Engineering, India, in 2000. He joined Schweitzer Engineering Laboratories, Inc. (SEL) in 2003 as an associate protection engineer in the engineering services division. He is presently working as a senior research engineer in SEL research and development. He was selected to participate in the U. S. National Academy of Engineering (NAE) 15th Annual U. S. Frontiers of Engineering Symposium. He is a senior member of the IEEE and currently has seven patents in the areas of power system protection, control, and fault location.

Previously presented at the 2016 Texas A&M
Conference for Protective Relay Engineers.

20160208 • TP6713-01